INTERFACE

rsif.royalsocietypublishing.org

Research

Cite this article: Meigel FJ, Alim K. 2018 Flow rate of transport network controls uniform metabolite supply to tissue. *J. R. Soc. Interface* **15**: 20180075.
http://dx.doi.org/10.1098/rsif.2018.0075

Received: 26 January 2018
Accepted: 10 April 2018

Subject Category:
Life Sciences–Physics interface

Subject Areas:
biophysics, biomechanics

Keywords:
transport networks, fluid flow, supply profile

Author for correspondence:
Karen Alim
e-mail: karen.alim@ds.mpg.de

Electronic supplementary material is available online at https://doi.org/10.6084/m9.figshare.c.4071710.

THE ROYAL SOCIETY PUBLISHING

Flow rate of transport network controls uniform metabolite supply to tissue

Felix J. Meigel and Karen Alim

Max Planck Institute for Dynamics and Self-Organization, 37077 Göttingen, Germany

KA, 0000-0002-2527-5831

Life and functioning of higher organisms depends on the continuous supply of metabolites to tissues and organs. What are the requirements on the transport network pervading a tissue to provide a uniform supply of nutrients, minerals or hormones? To theoretically answer this question, we present an analytical scaling argument and numerical simulations on how flow dynamics and network architecture control active spread and uniform supply of metabolites by studying the example of xylem vessels in plants. We identify the fluid inflow rate as the key factor for uniform supply. While at low inflow rates metabolites are already exhausted close to flow inlets, too high inflow flushes metabolites through the network and deprives tissue close to inlets of supply. In between these two regimes, there exists an optimal inflow rate that yields a uniform supply of metabolites. We determine this optimal inflow analytically in quantitative agreement with numerical results. Optimizing network architecture by reducing the supply variance over all network tubes, we identify patterns of tube dilation or contraction that compensate sub-optimal supply for the case of too low or too high inflow rate.

1. Introduction

Transport processes organized in network structures are ubiquitous in our life, from road traffic [1] and power networks [2] to river estuaries [3] and vascular systems of extended organisms [4,5]. In particular, fluid flow-driven transport through networks underlies many technological applications like fuel cells [6], micro-fluidic devices [7] or filtration systems [8] and their medical applications [9]. Most significantly, all higher forms of life rely on fluid flow-based transport networks to provide their tissues with metabolites like nutrients or minerals, as there are the circulatory system of animals [10], the plant xylem vascular system [11] and the hyphae networks of fungi [12–14]. Within a tissue, each cell needs to be provided with the same minimal amount of metabolites. How does a transport network need to be set up to make sure that metabolites arrive uniformly at each cell within a tissue? Here, we theoretically investigate the requirements on flow and network architecture for uniform supply.

On the level of inter-vascular tissue, models for minimal supply due to metabolite uptake and metabolite diffusion within the tissue date back 100 years to Krogh's model [15]. Yet, Krogh assumes that metabolites are provided by the vasculature at a constant rate at all vessel walls [16]. This strong simplification neglects that vascular network architecture and resulting asymmetries in flow-based transport give rise to large variations in metabolite availability within the network. On the level of the vascular network itself, studies mapping out variations in metabolite availability are scarce [17–19]. Insight into what controls uniform metabolite supply at the vasculature level is missing. Instead research has focused on network flow and not transport properties identifying scaling relationships regarding the network's fluid dynamics [20–27]. Another branch of theoretical models for vascular systems

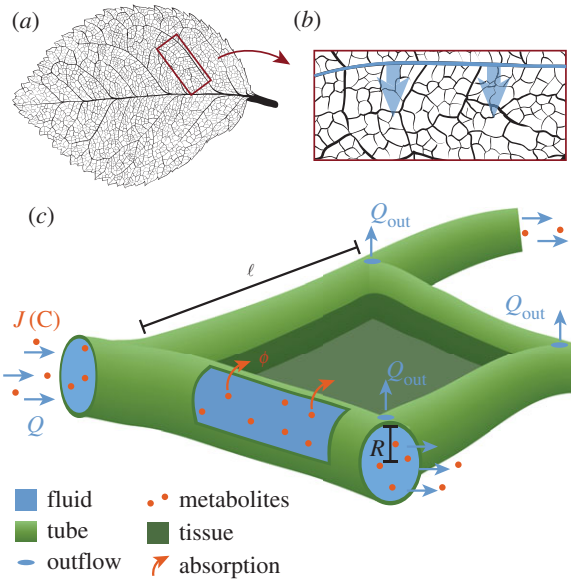

Figure 1. Schematic sketch of metabolite supply in leaves. (*a*) Vasculature of a leaf displaying the primary vein horizontally at the centre and secondary veins as next biggest veins departing from the primary vein, down to the highly inter-webbed higher order veins. (*b*) The secondary vein (thick blue) supplies the tubular higher order vein network with metabolites and fluid. (*c*) Xylem vessel network modelled as network of tubes of varying radius R and length ℓ. Inflow of fluid flow rate Q and metabolite flux J from upstream tubes (left). Fluid evaporation through stomata at the leaf surface modelled by constant outflow Q_{out} at every network node. Metabolites are advected and diffuse within the fluid. In addition, metabolites get absorbed ϕ along the tube wall into cells at a constant rate ν. (Online version in colour.)

investigated optimal network topologies with minimal transport cost in the form of dissipation [26,28,29]. Including robustness to damage or flow fluctuations [30,31] or vessel growth [32] in these studies resulted in network topologies in closer resemblance to observable vascular networks. However, despite the efforts to find minimal dissipation networks to understand transport networks in nature, it is not obvious that the efficiency of a transport network is what organisms optimize for. Instead, measurements on zebrafish vasculature suggest that biological transport networks maintain uniform partitioning of blood cells and thus uniform oxygen supply [33] and are not optimized for minimal dissipation. The vasculature architecture might, as established for tissue, be built for the uniform supply of metabolites like oxygen, nutrient compounds or biochemical signals. A further indication is that networks adapt to reinforce supply to tissues and organs [34].

The spread of metabolites through fluid flow is well described in hydrodynamics. Here, the transport of particles in a single long slender tube is efficiently captured by *Taylor dispersion* [35–37]. The important contributions of particle transport are advection by fluid flow and molecular diffusion, resulting in a decoupling of flow dynamics and particle concentration dynamics. Transport of particles that in addition get absorbed along the tube wall is well studied in the setting of heat conduction [38–41]. Yet, the concentration patterns of particles within a transport network are fundamentally more complicated due to the particle concentration being coupled in a global manner by the network spanning flow. Thus, further theoretical development is required as presented here.

Table 1. Nomenclature.

R	tube radius
ℓ	tube length
L	network length
N	number of tubes in the network
Q	fluid flow rate
U	fluid flow velocity
C	metabolite concentration
J	metabolite flux
κ	molecular diffusivity of metabolite
ν	absorption rate of metabolite
γ	absorption parameter; $\gamma = \nu/\kappa$
ϕ	overall absorption along a tube
$\hat{\phi}$	overall absorption capacity along a tube
Pe	Péclet number, ratio of diffusive and advective timescale
S	ratio of the timescales for absorption
β	concentration decay constant

While a hydrodynamic perspective provides a general picture with a minimum of assumptions and hence a broad applicability, the specifics of metabolite flow differ between biological systems. In light of network optimization approaches [30–32], we apply the general hydrodynamic perspective to the tissue specifics of plant leaf xylem vessels in dicotyledons. In plants, the transport of water and metabolites, especially soil-bound nutrients and minerals like nitrate or potassium [11], from the plant roots to the leaf tissue is routed in highly pitted and rigidly lignified xylem veins [42]. Xylem veins should not be confused with the oppositely routed phloem veins predominantly transporting sugar away from the leaf tissue [43,44]. We consider the spread of the scarce metabolites in xylem fluid as limiting for maintaining the function of leaf cells and thus focus on the xylem network neglecting the detailed spreading dynamics of metabolites within the tissue itself. Metabolites enter leaf cells dominantly at the level of inter-webbed higher order veins, while the primary and secondary order veins distribute metabolites over the large scale of the leaf [45]. Here, we focus on a leaf tissue excerpt pervaded by higher order veins. A secondary vein is the source of metabolite-enriched fluid flowing through higher order vessels pervading the leaf tissue (figure 1*a*,*b*). Fluid flow is regulated through evaporation control across the entire leaf blade [46]. Evaporation is commonly modelled by a constant outflow of fluid at every node within the vascular network [30,31], for details see electronic supplementary material S1. Metabolites are absorbed continuously along the walls of the tubular vessels into the tissue supplying the cells there (table 1).

In this paper, we develop a theoretical framework to optimize flow dynamics and architecture of transport networks for uniform supply of metabolites to surrounding tissues focusing exemplarily on plant xylem networks. We derive analytical expressions for the absorption of metabolites within a single tube and use these results to simulate supply patterns in the inter-webbed transport networks. We find that the inflow rate is the dominant factor

controlling supply patterns for all network architectures. For low inflow rates, average fluid velocities are small and metabolites are mainly absorbed next to the flow inlets. For high inflow rates, average velocities are fast and metabolites are mainly absorbed at the far end opposing the inlets. In between, we identify an optimal inflow rate that yields uniform absorption and thus supply levels. We present a one-dimensional network analogue that allows us to derive an analytical expression for the optimal flow rate as a function of system parameters such as network size and average tube radius in agreement with simulations. Further optimizing the network architecture for low, optimal or high inflow rate, we find that localized adaptation in tube radius is capable of compensating for the non-uniform supply patterns at low and high inflow rate, yet cannot outcompete the optimal inflow rate.

2. Results

2.1. Metabolite absorption across a fluid-filled tube

Consider a cylindrical tube filled with fluid flowing at flow velocity $U(r,z)$ along the tube. Metabolites are advected with the flow and in addition disperse due to molecular diffusion with diffusivity κ. Considering the small scales of xylem vessels and xylem flow, we are in the regime of low Reynolds number, where flow is best described by laminar Poiseuille flow. Thus, we describe the flow along the longitudinal axis z varying in radial direction r in the circular tube with a radius R and length ℓ as, $U(r,z) = 2(1 - r^2/R^2)\langle U(z)\rangle_r$. Here, $\langle U\rangle_r$ denotes the cross-sectionally averaged longitudinal velocity. The spread of metabolites of concentration C is thus fully described by

$$\frac{\partial C}{\partial t} + U(r,z)\frac{\partial C}{\partial z} = \kappa\left[\frac{1}{r}\frac{\partial}{\partial r}\left(r\frac{\partial C}{\partial r}\right) + \frac{\partial^2 C}{\partial z^2}\right]. \tag{2.1}$$

Metabolites are absorbed into the surrounding tissue along the tube wall, given by the boundary condition

$$\kappa\frac{\partial C}{\partial r}\bigg|_{r=R} + \nu C(R) = 0, \tag{2.2}$$

analogous to heat absorption or surface reactions. Here, the parameter ν denotes the metabolite absorption rate at the tube wall. Dividing ν by the molecular diffusivity, we define the absorption parameter γ, where we consider ν as a constant tissue property. According to [38], the advection–diffusion equation, equation (2.1), can be reformulated employing both the boundary condition equation (2.2) and the Poiseuille profile as a single absorption–advection–diffusion equation in cylindrical coordinates.

In analogy to the derivation of *Taylor dispersion* by Taylor [35], a simpler, though approximated, expression is possible where the concentration dynamics only depend on the longitudinal coordinate z. To this end, the metabolite concentration is separated into the sum of a cross-sectional average concentration $\langle C\rangle_r$ and the radial variation C', $C(r,z) = \langle C(z)\rangle_r + C'(r,z)$. The multidimensional diffusion–advection for $C(r,z) = \langle C(z)\rangle_r + C'(r,z)$ can be simplified to an equation for the cross-sectionally averaged concentration $\langle C(z)\rangle_r$ if the cross-sectional variations of the concentration $C'(r,z)$ are much smaller than the averaged concentration itself [35,47], resulting in

$$\frac{\partial\langle C\rangle_r}{\partial t} = -\frac{2\kappa}{R^2}\frac{4\gamma R}{4+\gamma R}\langle C\rangle_r - \frac{12+\gamma R}{12+3\gamma R}\langle U\rangle_r\frac{\partial\langle C\rangle_r}{\partial z} + \left(\kappa + \frac{12+\gamma R}{12+3\gamma R}\frac{\langle U\rangle_r^2 R^2}{48\kappa}\right)\frac{\partial^2\langle C\rangle_r}{\partial z^2}. \tag{2.3}$$

This approach employs three approximations. First, the timescale of diffusion across the tube's cross section has to be much smaller than the timescale of advection, $\ell/\langle U\rangle_r \gg R^2/\kappa$. This sets an upper bond for the later choice of the fluid inflow rate. The second assumption states that the cross-sectional variations of the concentration have to be small $\langle C\rangle_r \gg C'$. As a high absorption parameter γ implies a large concentration gradient across the cross section, the second assumption implies $\gamma R \ll 1$. Third, the variation of C' has to be much greater in radial direction than in flow direction $\partial_r^2 C' \gg \partial_z^2 C'$. The last assumption implies the tube radius to be smaller than its length $R \ll \ell$. This is fulfilled by long slender tubes.

Employing these assumptions, the cross-sectional average metabolite concentration along a tube in steady state is given by an exponential decay from initial concentration C_0,

$$\langle C(z)\rangle_r = C_0\exp\left(-\beta\frac{z}{\ell}\right) \text{ and}$$
$$\beta = \frac{24\cdot \mathrm{Pe}}{48 + R\gamma\cdot \mathrm{Pe}/S}\left(\sqrt{1 + 8\cdot\frac{S}{\mathrm{Pe}} + \frac{3}{4}\cdot R\gamma} - 1\right). \tag{2.4}$$

Here, we introduced two-dimensionless variables Pe and S. $\mathrm{Pe} = \langle U\rangle_r\ell/\kappa$ is the well-known Peclet number describing the relation between diffusive and advective timescale. S is the ratio of the timescale for absorption, given by the product of the dimensionless absorption parameter and time to diffuse across the tube's cross section, and the time to be advected out of the tube, resulting in $S = \gamma\kappa\ell/R\langle U\rangle_r$.

Considering a constant influx J_0 by advection and diffusion of metabolites at the tube's start, we find that the initial concentration C_0 is given by

$$C_0 = \frac{J_0}{\langle U\rangle_r + \kappa(\beta/\ell)}. \tag{2.5}$$

The overall absorption ϕ along a tube is given by the integrated flux of metabolites across the tube wall $\mathcal{W}$, $\phi = 2\pi R\int_{\mathcal{W}}\kappa\nabla C\,\mathrm{d}z$, where $\mathrm{d}z$ is integrating over the length of the tube. As in the derivation of the effective diffusion–advection–absorption equation equation (2.3), we use $R\gamma \ll 1$ to arrive at

$$\phi = \pi R^2 J_0 4\frac{S}{\mathrm{Pe}}\left(48 + \frac{R\gamma\cdot\mathrm{Pe}}{S}\right) \times\frac{(48 - (R\gamma\cdot\mathrm{Pe}/S)(\Lambda-2))}{48(48 + \gamma R\cdot\mathrm{Pe}/S + 24(\Lambda-1))\cdot(\Lambda-1)} \times\left(1 - \exp\left(-24\cdot\mathrm{Pe}\cdot\frac{\Lambda-1}{48+\gamma R\mathrm{Pe}/S}\right)\right), \tag{2.6}$$

where Λ is an abbreviation $\Lambda = \sqrt{8S/\mathrm{Pe} + 3/4\gamma R + 1}$. We identify two factors that control the absorption in a tube. The first is the total influx of metabolites over the cross-sectional area of the tube $\pi R^2 J_0$. The total influx of metabolites is the upper limit for absorption in the tube. The second factor is the tube's capacity to absorb metabolites as $\hat{\phi} = \phi/\pi R^2 J_0$ with $\hat{\phi} \in [0,1]$. This absorption capacity is independent of the concentration of metabolites and only depends on the parameters of the tube and the flow velocity within the tube.

For the derivation of the optimal inflow rate, it is essential to approximate the absorption capacity as resulting from equation (2.6). We initially approximate the inverse of the absorption capacity $\hat{\phi}^{-1}$ by taking a finite $\mathrm{Pe} > 0$ and using $R\gamma \ll 1$ to find $\hat{\phi}^{-1} = 1/2S + 1$. Resubstituting the system's parameters for S, we find for the absorption capacity of a tube

$$\hat{\phi} = \frac{2\gamma\kappa\ell}{R\langle U\rangle_r + 2\gamma\kappa\ell}. \tag{2.7}$$

Note the simple dependence of the absorption capacity on the cross-sectionally average flow velocity in the tube. The approximation of the absorption capacity has been verified numerically to hold over the parameter space considered here, see electronic supplementary material S4. Note that this simplified expression is only used for the analytical derivation of the optimal inflow rate. For simulations, the full expression equation (2.6) is used. From now on, we drop the brackets $\langle\rangle_r$ and only refer to cross-sectional averaged observables.

2.2. Absorption patterns in fluid flow-driven transport networks

In a transport network, individual tubes are connected at nodes. Here, we aim to model the geometry of higher order xylem veins branching from a second order vein in dicotyledons, as shown in figure 1*b*. We choose a planar transport network representing a rectangular excerpt of the leaf tissue. For the tissue excerpt we choose a general vascularization using a slightly randomized tessellation of space, where the network is built with small triangles, known to bear least artefacts [30]. A small Gaussian noise of a twentieth tube length ℓ is added to the positions of the tessellation nodes to avoid pattern artefacts arising from the underlying topology otherwise, see electronic supplementary material S2. The tube length varies accordingly in a normal distribution around the mean tube length $\langle\ell\rangle$. In agreement with observations of diminishing hierarchy in the higher interwebbed xylem vessel radii [20,48], we set the same radius R for all tubes. Fluid and metabolites are flowing into the network at network nodes along one side of the rectangular region, representing the supply from secondary veins into the tissue. Xylem vessels are organized in vascular bundles in lower order veins that branch out into the interwebbed higher order xylem network [49] presumingly supplying the same flow at every inflow node. Therefore, we approximate inflow rates Q_{in} to be equal at all inflow nodes. To represent the effect of fluid evaporation at stomata, fluid, but not metabolite, is flowing out at every node in the network Q_{out} (figure 1*c*). Metabolites are absorbed across each tube wall. The absorption rate ν is constant throughout the network. Yet, as we have learned by studying a single tube in the previous section, the amount of metabolite absorbed depends on how much metabolite is available in the fluid, and how much time the metabolite has to travel to the tube wall to get absorbed. Therefore, absorption despite a constant absorption rate varies largely within a network.

The flow of the metabolites is determined by the fluid flow in accordance with equation (2.1). The fluid flow throughout a network is fully defined by the network's architecture, the inflow and outflow rates and Kirchhoff's circuit law. The cross-sectionally averaged fluid flow velocity in a tube follows subsequently from pressure drops $\Delta P = R_{\mathrm{hyd}} \cdot Q$ along the tube. Each tube is considered as straight cylinder with hydraulic conductance of $K_{\mathrm{hyd}}^{-1} = (8/\pi)\ell\eta(1/R^4)$, where η denotes the dynamic fluid viscosity. The pressure at every node is calculated by multiplying the inverse of the network conductivity matrix with the inflow or outflow rates at every node. The pressure drop along the tube is the difference between the pressure values at the start and end node. The fluid flow is solved consistently through the whole network and takes network geometry and viscous and friction forces via the hydraulic resistance into account. Considering steady-state solutions, the flow does not fluctuate over time.

The absorption of metabolite across a tube's wall within the network depends on the metabolite available and the tube's absorption capacity. The absorption capacity of the tube follows directly from each tube's physical parameters and the fluid flow velocity within the tube. Next, we need to calculate the influx of metabolites J_0 in every tube which we solve iteratively throughout the network starting with the influx nodes, see electronic supplementary material S3A. For simplification, we focus on stationary, steady-state absorption patterns. We employ that metabolite flux is conserved at every network node. All metabolites flowing into a node are redistributed into tubes originating from this node. Redistribution is proportional to diffusion and flux into each tube. The metabolite outflux at the end of a tube is then given by the difference in metabolite influx and total absorption along the tube. Finally, at the lower end of the considered network excerpt, opposite the inflow nodes, remaining metabolites are flowing out of the network. As the outflowing metabolites would lead to an accumulation of metabolites, we state the amount of metabolites not absorbed for every considered network excerpt.

Taking our initial motivation from plant leaves, we choose an average tube length $\ell = 0.1$ mm and tube radius $R = 3\,\mu$m in accordance with xylem vessels [20,21,50]. Note that there is a difference between leaf vein and xylem vessel radius, as leaf veins bundle both phloem and xylem vessels. We thus consider xylem vessels to be less than half the radius of leaf veins in our parameter choice. The order of magnitude of the total inflow rate is chosen to yield velocities observable in lower order xylem vessels $\langle U\rangle_r \approx 1\,\mu\mathrm{m\,s^{-1}}$. We vary the fluid inflow rate between $Q_{\mathrm{in}} = 0.8 \times 10^{-6}\,\mathrm{mm^3\,s^{-1}}$ to $Q_{\mathrm{in}} = 6.4 \times 10^{-6}\,\mathrm{mm^3\,s^{-1}}$. The choice of the inflow is consistent with a average water evaporation of approximately $0.1\,\mathrm{mol\,m^{-2}\,s^{-1}}$ [42,51] and an average stomata density of $200\,\mathrm{mm^{-2}}$ [52]. For the molecular diffusivity, we consider small molecules with $\kappa = 1 \times 10^{-10}\,\mathrm{m^2\,s^{-1}}$. For the network size, we choose a triangulation with $\mathcal{N} \approx 1000$ tubes. As xylem vessels consist of highly pitted dead lignified tissue, no active absorption by chemical reactions but passive absorption by membrane permeation is expected. Values for membrane permeation are typically in the range of $\nu \approx 1 \times 10^{-9}$ m [53] and depend on both membrane and metabolite properties. Alternatively an estimation for the absorption parameter γ can be derived from concentration profiles in xylem veins [54]. Translating the measured exponential decay for higher order veins, we find $\gamma \approx 10\,\mathrm{m^{-1}}$ [54,55]. This estimate for γ is in accordance with estimates using membrane permeation. Thus, for the numerical calculations an absorption parameter of $\gamma = 10\,\mathrm{m^{-1}}$ is chosen. Revisiting the three assumptions made in equation (2.3), we verify that these assumptions hold for the chosen network topologies, see electronic supplementary material S4.

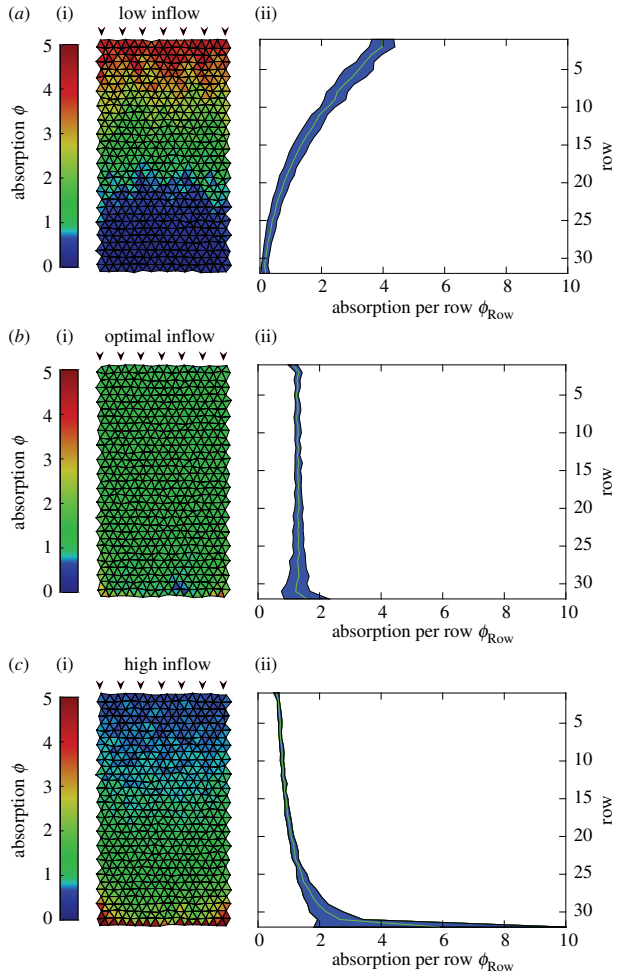

Figure 2. Supply patterns are controlled by fluid inflow rates. Supply pattern of a rectangular tissue section pervaded by a transport network for increasing fluid inflow rate ranging from (*a*) $Q_{in} = 0.8 \times 10^{-6}\,\mathrm{mm^3\,s^{-1}}$, via (*b*) $Q_{in} = 3.2 \times 10^{-6}\,\mathrm{mm^3\,s^{-1}}$, to (*c*) $Q_{in} = 6.4 \times 10^{-6}\,\mathrm{mm^3\,s^{-1}}$. The transport network is built of tubes of equal radius and roughly equal length triangulating the tissue section under consideration. Metabolites are absorbed across tube walls into the tissue. (*a*(i),*b*(i),*c*(i)) Supply pattern in every triangulated tissue section given by the average metabolite absorption along neighbouring tubes. The absorption is normalized with the inverse of the total influx J_{tot}^{-1} and the total number of tubes $\mathcal{N}$. (*a*(ii),*b*(ii),*c*(ii)) Standard deviation and mean absorption per row counting downward from the inflow nodes at the top of the network. At low inflow rates (*a*) metabolites are absorbed close to inflow and are not transported through the network while for high inflow rates (*c*) metabolites get flushed through the network for being absorbed mainly at the end. The variance in absorption across all tubes is 0.75 for the low inflow rate and 2.35 for the high inflow rate. In between these two cases, an optimal inflow rate with the lowest variance exists (*b*) that yields uniform supply and an overall variance of only 0.07. Remaining metabolites are flowing out at the bottom end amounting to 0.6%, 4.2% and 19.4% of the metabolite influx for (*a*), (*b*) and (*c*), respectively. (Online version in colour.)

We first study metabolite supply patterns in uniform transport networks, where all tubes have the same radius R. To compare different inflow rates, we normalize the absorption by the total influx of metabolites. We find that the total fluid inflow rate is dominating the supply patterns (figure 2). For small inflow rate, average flow velocities in the network are slow and the highest absorptions is near the inflow nodes. Metabolites are not transported through to the end of the network limiting supply there. Calculating the mean absorption per row ϕ_{row} from inflow to the opposing end, we can characterize this regime by $\phi_{row} > \phi_{row+1}$ (figure 2*a*(ii),*b*(ii),*c*(ii)). For high inflow rates, average flow velocities are fast and the absorption increases with the distance from the inflow nodes $\phi_{row} < \phi_{row+1}$. Metabolites arrive at the end of the network too quickly before getting absorbed limiting supply close to the inflow nodes. Between these limiting cases, we identify an inflow rate that gives rise to an optimally uniform supply pattern. We define the optimum by the lowest variance. The variance is calculated over the ensemble of all tubes. The overall variance in the optimal case is 0.07 compared to 2.35 and 0.75 in the examples of low and high inflow rate, respectively, shown in figure 2. In the optimally uniform supply pattern, absorption is the same constant rate in subsequent rows, $\phi_{row} = \phi_{row+1}$. On the basis of this simple relation stating uniform absorption, a scaling law for the optimal inflow rate is derived next.

2.3. Scaling law for the optimal inflow rate

To derive a scaling law for the optimal inflow rate that gives rise to the most uniform supply pattern, we consider a one-dimensional toy model of connected single tubes that captures the essential flow and transport characteristics along the rows of the two-dimensional transport networks investigated above. For this, we look at a straight pipeline of N identical tubes. As for the networks considered in the previous section (figure 2), all tubes are of the same radius R and length ℓ, in accordance with observations of diminishing radius hierarchy in higher order veins [20,48]. Metabolites and fluid are flowing into the first tube Q_{in} and fluid is leaving at a constant rate Q_{out} at every node between adjacent tubes. Metabolites cannot exit at nodes but remain in the fluid until the very end of the pipeline or are absorbed. Also the fluid inflow rate and total fluid outflow rate are equal, i.e. $Q_{out} = Q_{in}/N$. This results in a constant decrease in flow rate by Q_{in}/N from one tube to the subsequent. To translate this to cross-sectionally averaged flow velocities, which are the flow properties determining absorption, we use $U = Q/\pi R^2$. Consequently, the flow velocity in segment $m+1$ is given by $U_{m+1} = U_m - Q_{in}/\pi R^2 N$.

The outflux of metabolites from one tube is equal to the influx of metabolites in the subsequent tube $J_{out,m} = J_{in,m+1}$, as all tubes have the same radius R. If $\pi R^2 J_0$ is the total amount of metabolites flowing into the first tube, then only the fraction $1 - \hat{\phi}_1$ is flowing out while the fraction $\hat{\phi}_1$ is absorbed. Generalizing we determine the absorption in tube m as

$$\phi_m = \pi R^2 J_0 \hat{\phi}_m \prod_{j=1}^{m-1} (1 - \hat{\phi}_j). \tag{2.8}$$

The state of optimally uniform absorption is now defined by absorption in subsequent tubes being equal. We use this constraint to determine the inflow rate that corresponds to the optimally uniform supply pattern. Using equation (2.8) to write the absorption in the $m+1$ tube as a function of the absorption in the previous tube and inserting the equality constraint, we arrive at an expression including absorption capacities only, $(1 - \hat{\phi}_m)\hat{\phi}_{m+1} = \hat{\phi}_m$. Inserting the simplified expression for the absorption capacity from equation (2.7), we find the scaling law determining the optimal inflow rate

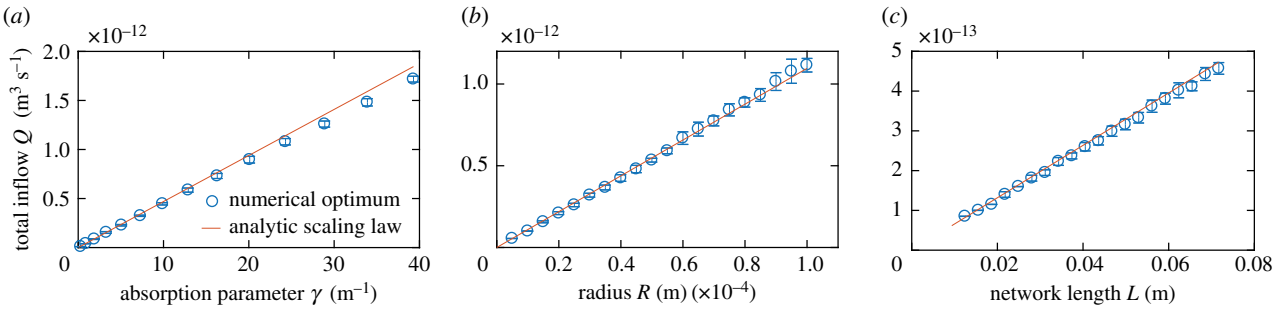

Figure 3. Scaling of the optimal inflow rate for uniform supply of a two-dimensional rectangular tissue section with system parameters. The optimal inflow rate defined as lowest overall variance in absorption scales linearly with the absorption parameter γ (*a*), the total network length L (*b*) and the tube radius R (*c*). While one parameter was varied, the other parameters were kept constant. Error bars represent the standard deviation over 15 independent runs. Data are in agreement with the scaling law (red line) of the optimal inflow rate derived for a one-dimensional toy model and adapted to two-dimensions by a geometrical factor.

to yield uniform absorption

$$Q_{\text{in}} = 2\pi\kappa\gamma LR, \tag{2.9}$$

where $L = N\ell$ denotes the length of the sequence of pipes. Note that this condition is independent of which tube segment m is considered. The absorption is uniform along the entire sequence of tubes.

Our toy model is set up to capture the essential flow and transport characteristic along the rows of a two-dimensional network excerpt modulus a geometrical factor. To confirm that the same functional dependence of the optimal inflow rate holds for two-dimensional networks, we return to our simulations of rectangular two-dimensional networks. For a given parameter choice, we vary the inflow rate and determine its optimal value by the minimal variance in absorption. We independently vary the absorption parameter γ and the tube radius R, equal for all tubes right now, as well as the overall size of the network L (figure 3). While one parameter was varied, the other parameters were kept constant. To cover a large parameter range, base parameter values are chosen as $\ell = 0.1$ mm, $R = 3\,\mu$m and $\gamma = 10\,\text{m}^{-1}$, see electronic supplementary material S5. For each parameter combination, the inflow rate was varied in step sizes of $\Delta Q = 1.5 \times 10^{-6}\,\text{mm}^3\,\text{s}^{-1}$. Note, to increase the overall size of the network, additional nodes where added. Therefore, Q_{out} decreased, and thus the overall flow velocity gradient decreased. Each run over a parameter combination was repeated 15 times with different random Gaussian node perturbations of a rectangular two-dimensional network with tubes of the same radii R. We find a linear scaling between the optimal inflow rate and the absorption parameter, the radius, and the overall size of the network in agreement with the scaling law's prediction. Even more, if we multiply the optimal inflow rate derived above for the one-dimensional tube network by a geometrical factor Γ taking into account the two-dimensional network geometry, the numerical results follow exactly the analytical prediction. The geometrical factor is a product of three terms $\Gamma = \Gamma_{\text{L}} \cdot \Gamma_{\text{AR}} \cdot \Gamma_{\text{IF}}$, where the first term is correcting the length of the network and the later two are needed to correctly link the velocity profiles with the inflow in the network. The total length of the network in flow direction is effectively shortened as tubes of the two-dimensional network are not connected with an angle of 180° as in the toy model, but the network is a tessellation of approximately equilateral triangles. The length of the network has thus to be shortened corresponding to the ratio of height and side length of such a triangle with $\Gamma_{\text{L}} = \sqrt{2}/3$. Considering the rows of nodes, the inflow of fluid in 16 nodes is distributed to 17 nodes in the next row. The flow in tubes connecting these two layers of nodes is thus reduced by the ratio $\Gamma_{\text{AR}} = \frac{16}{17}$. As the total inflow is the inflow over the complete width of the network, the optimal inflow has to flow into every two to three tubes connected to the 16 inflow node giving rise to $\Gamma_{\text{IF}} = 47$.

2.4. Optimization of network architecture for uniform supply

We found that a global change in the total fluid inflow rate is the most important control mechanism to generate uniform supply patterns in a tissue pervaded by a transport network. How does a network architecture need to change to compensate low or high inflow rates? How much more can we minimize the variance in absorption even if the fluid flow rate is optimal? To answer these questions, we now optimize our previously found supply patterns by allowing for local dilation or contraction of tubes starting with the randomized networks introduced above. In addition to tube dilation and contraction, changes to the network architecture by discarding entire tubes are allowed. A tube is regarded as cut, if its radius is reduced below a threshold of 0.05 µm, compared to an average tube radius of $R = 3\,\mu$m. While locally changing the network architecture, we keep the total amount of material $M = \sum_i R_i \ell_i$ within the network constant as we redistribute changes in M over all radii equally. For this, we numerically optimize the network topology using Monte Carlo methods, explained in detail in electronic supplementary material S3B.

We optimize the network architecture regarding uniform tissue supply for the cases of low, high and optimal inflow rate (figure 4). In all three cases, overall variance in absorption was successfully decreased. For low inflow rates, we observe a contraction of tubes near the influx nodes and an expansion of tubes towards the opposing end. Contraction of tubes speeds up flow velocities thus reducing otherwise dominating absorption close to the inflow nodes and thereby making metabolites available for absorption further onwards. The increase in absorption follows spatially the rapid increase in radius. This indicates that shifts in the radius distribution impact the local absorption profile strongly. For high inflow rates, we observe the opposite optimization mechanism.

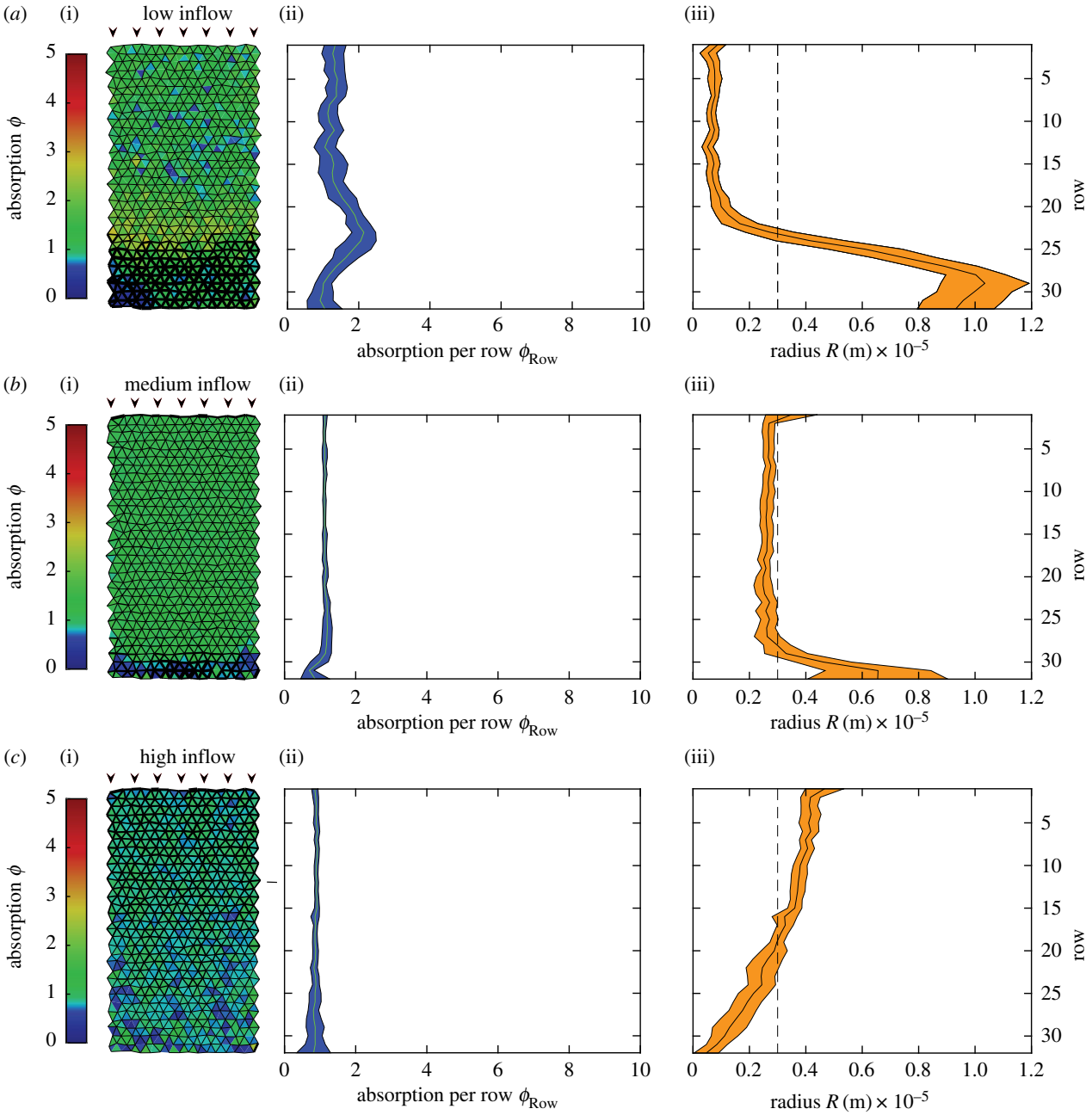

Figure 4. Optimized network architectures for uniform metabolite supply patterns. Supply pattern for the same low (*a*), optimal (*b*) and high (*c*) inflow rate as in figure 2 but optimized network architecture. (*a*(i),*b*(i),*c*(i)) Supply pattern in every triangulated tissue section given by the average metabolite absorption along neighbouring tubes, see also figure 2. Thickness of tubes represents the tube radius. (*a*(ii),*b*(ii),*c*(ii)) Standard deviation and mean absorption per row counting downward from the inflow nodes at the top of the network. (*a*(iii),*b*(iii),*c*(iii)) Standard deviation and mean radius per row. Dashed line marks average tube radius. (*a*) For low inflow rate tubes contract near inflow nodes, speeding up flows there and thus propagating metabolites further down the network. Tubes dilate towards the network end further increasing absorption there. Variance in absorption is reduced to 0.211. (*c*) For high inflow rate tubes dilated close to the inflow nodes, slowing down flow there and thus increasing absorption. Variance is reduced by two orders of magnitude to 0.040. (*b*) Also for the optimal flow rate variance in absorption is reduced to 0.030. Note, that although metabolite outflux is penalized, it only decreased for (*b*) to 1.9% and increased for (*a*) to 1.9% and (*c*) to 29.0%. Note, that no edges were cut. (Online version in colour.)

Tubes dilate close to the inflow and contract towards the opposing end. Here, dilation decreases flow rate and increases the absorption early on, while at the same time reducing the amount of metabolite flushing through. For the optimal inflow rate, we observe slight dilation near the inflow and near the outflow nodes. These changes correct for network artefacts arising from the chosen rectangular form of the excerpt. In all optimized networks, we find small fluctuations in the absorption pattern which result from the randomized node positions and random tube lengths.

3. Discussion

We investigated what is needed to achieve a uniform supply rate of metabolites to tissue via a tubular transport network. We find that the fluid inflow rate is the most important control mechanism. We give an analytical scaling law for the optimal inflow rate as a function of system parameters. Yet, even if the optimal inflow rate is not available, altering the network geometry by dilating or contracting certain tube radii can reduce the overall variance in supply by an order of magnitude.

Optimizing for uniform supply rate across a transport network is a novel perspective regarding the theoretical investigation of optimal transport networks, where the focus is mainly on minimizing total dissipation $P = \sum_i Q_i^2/K_{hyd,i} = \sum_i \pi \langle U \rangle_i^2 \eta \ell_i$ [30,31,56,57]. For comparison, we compute the total dissipation for our example network shown in figures 2 and 4. For the networks of equal radii, we find that the dissipation for the optimal inflow rate is of the same order of magnitude to hundredfold higher than for the less uniform supply patterns arising from low and high inflow rates, respectively. Optimizing the network architectures to enhance uniform metabolite supply even increases total dissipation for low and optimal inflow rate, while dissipation is only slightly decreased for high inflow rates. We conclude that total dissipation and uniform metabolite supply are orthogonal properties regarding transport networks. It could well be that biological transport networks balance both properties by optimizing them at the same time. Yet, we observe the differentiation of biological transport networks into different types of tubes like lower order versus higher order veins. This suggest that biological transport networks could be divided into parts that are targeted at transport costs, others targeted at mechanical structures, and others targeted at supply.

We find that the inflow rate into a tissue has the biggest impact on how uniform supply is throughout the tissue. For plants, sub-optimal environments, such as a drought, lead to a reduction in water flow. Following our results, a change in the inflow rate will result in a change in the supply pattern, even if the same amount of metabolite is still available. Plant leaves can actively control fluid flow rates by managing evaporation via opening and closing of stomata. It is inspiring to note that therefore plants could control, to some extent, for optimal inflow rates. Unfortunately, to our knowledge, no data on flow rates in leaf veins is available to test this. Alternatively, we find that specific patterns of vein radii could also compensate sub-optimal inflow. Though the adaptation of xylem veins on drought conditions has received general attention, see e.g. [58–61], it has not been investigated to what extent plants modify the hierarchy of higher order xylem vessel radii for compensatory patterns when grown in sub-optimal conditions. Although our findings predict the regulation of the flow rate by stomata control to be the dominant mechanism, it would be fascinating to check for radii patterns in higher order vessels with established means of vessel network analysis [48].

We investigated uniform metabolite supply by xylem vein vasculature focusing on two dimensions. On the level of modelling metabolite absorption on vessel walls, our framework can readily be extended to network topologies embedded in a three-dimensional space. That said, the dynamics of metabolite supply within the tissue surrounding the vessel walls changes dramatically if we go from two to three dimensions, simply because the physical space to be supplied increases. The spatial distribution of metabolite concentration in the tissue can be resolved by an explicit treatment of the reaction–diffusion dynamics in the extravascular space. Here, for example the Krogh formalism allows this computationally complex task to be reduced to the spacing between vessels as an additional parameter [15,16]. To our knowledge the concept of Krogh radii has yet not been considered in plant tissue. As we consider flat leaves, we restricted our analysis here to two dimensions. We studied vascular networks with biological observed vessel spacing of $\langle \ell \rangle \approx 0.1$ mm in our model, assuming that metabolite spread for these physiological values is not limited within the tissue but rather limited by the supply through the vasculature. As we investigate uniform supply patterns the variation in absorption rates of neighbouring vessels is by definition very small, also limiting supply variations in the tissue.

As leaf vascular specifics have been incorporated in our model using a distinct source and sink distribution on the network level, the derived scaling law is only applicable to higher order xylem vessel networks. However, the chosen hydrodynamic perspective of the metabolite spread through a vascular system considers only few assumptions and thus also allows for board applicability in other biological systems. As such, the absorption along a tube can be discussed in the setting of capillary beds in animal vasculature. Here, metabolites may be actively transported across the vessel wall with potentially nonlinear reaction kinetics that we in this work only approximate by a linear absorption parameter. More importantly, vessels are so small that blood flows in a plug flow and not Poiseuille flow. In our theoretical work, Poiseuille flow is the key to generate the fast mixing of metabolites across a tube, which is impaired in the pure plug flow. However, blood cells being squeezed through the tiny vessel create turbulent eddies and recirculation zones in the flow, which drive fast mixing across a vessel [16]. Based on fast mixing, our results may very well be applicable to capillary beds. For capillary beds, inflow rates are at first approximation a function of heart rate and the allocation of fluid along the hierarchical circulatory system. However, capillary beds also auto-regulate their flow by dilating or contracting so-called sphincters situated at the inflow nodes that dilate or contract the capillaries close by [16]—a control mechanism in agreement with our findings. Note that in this example even the location of compensatory regulation close to the inflow follows the predictions of our hydrodynamic model.

Taken together the evidence of control mechanisms in plant and animal vasculature, albeit scarce, suggests that indeed uniform supply might very well be targeted at the level of higher order veins and capillary beds. Our scaling law predicts a simple relationship between inflow rate and tissue size or vessel radius. Thereby, we pave the way for experimentally investigating supply patterns in biological transport networks.

Transport networks are at the basis of not only biological organisms but also technological design and medical applications. Investigating what properties make a transport network give rise to uniform supply, we identify the most important control mechanism, mainly inflow rate and secondary vessel diameter close to inlets. These controls may be important for so many more transport systems than the ones exemplified here. But most importantly, it sheds light on our understanding of the *transport* dynamics and not just fluid flow profiles in transport networks.

Data accessibility. This article has no additional data.

Authors' contributions. F.J.M. and K.A. designed and, performed research and wrote the paper.

Competing interests. The authors declare no conflict of interests.

Funding. This research was supported, in part, by the Deutsche Forschungsgemeinschaft (DFG) via grant no. SFB-937/A19 and the Max Planck Society.

Acknowledgements. We thank M. P. Brenner and P. Cha for their initial discussions about absorption in single tubes.

References

1. Sen P, Dasgupta S, Chatterjee A, Sreeram PA, Mukherjee G, Manna SS. 2003 Small-world properties of the Indian railway network. *Phys. Rev. E* **67**, 036106. (doi:10.1103/PhysRevE.67.036106)
2. Rohden M, Sorge A, Timme M, Witthaut D. 2012 Self-organized synchronization in decentralized power grids. *Phys. Rev. Lett.* **109**, 064101. (doi:10.1103/PhysRevLett.109.064101)
3. Rodriguez-Iturbe I, Rinaldo A. 1997 *Fractal river basins: chance and self-organization*. Cambridge, UK: Cambridge University Press.
4. Netti PA, Baxter LT, Boucher Y, Skalak R, Jain RK. 1997 Macro- and microscopic fluid transport in living tissues: application to solid tumors. *AIChE J.* **43**, 818–834. (doi:10.1002/aic.690430327)
5. Kapellos GE, Alexiou TS, Pavlou S. 2015 Chapter 8—Fluid–biofilm interactions in porous media. In *Heat transfer and fluid flow in biological processes* (eds SM Becker, AV Kuznetsov), pp. 207–238. Boston, MA: Academic Press.
6. Ma L, Ingham D, Pourkashanian M. 2005 16—Application of fluid flows through porous media in fuel cells. In *Transport phenomena in porous media III* (eds D Ingham, I Pop), pp. 418–440. Oxford, UK: Pergamon.
7. Santini JT, Cima MJ, Langer R. 1999 A controlled-release microchip. *Nature* **397**, 335–338. (doi:10.1038/16898)
8. Tufenkji N, Elimelech M. 2004 Correlation equation for predicting single-collector efficiency in physicochemical filtration in saturated porous media. *Environ. Sci. Technol.* **38**, 529–536. (doi:10.1021/es034049r)
9. Levey AS *et al.* 2009 A new equation to estimate glomerular filtration rate. *Ann. Intern. Med.* **150**, 604–612. (doi:10.7326/0003-4819-150-9-200905050-00006)
10. Isogai S, Horiguchi M, Weinstein BM. 2001 The vascular anatomy of the developing zebrafish: an atlas of embryonic and early larval development. *Dev. Biol.* **230**, 278–301. (doi:10.1006/dbio.2000.9995)
11. Choat B, Munns R, McCully M, Passioura J, Tyerman S, Bramley H, Canny M. 2010 Water movement in plants. In *Plants in action* (eds B Choat, R Munns), ch. 3. Melbourne, Australia: Australian Society of Plant Scientists. See http://plantsinaction.science.uq.edu.au/content/chapter-3-water-movement-plants.
12. Boddy L, Hynes J, Bebber DP, Fricker MD. 2009 Saprotrophic cord systems: dispersal mechanisms in space and time. *Mycoscience* **50**, 9–19. (doi:10.1007/S10267-008-0450-4)
13. Tero A, Takagi S, Saigusa T, Ito K, Bebber DP, Fricker MD, Yumiki K, Kobayashi R, Nakagaki T. 2010 Rules for biologically inspired adaptive network design. *Science* **327**, 439–442. (doi:10.1126/science.1177894)
14. Heaton LLM, López E, Maini PK, Fricker MD, Jones NS. 2012 Advection, diffusion, and delivery over a network. *Phys. Rev. E* **86**, 021905. (doi:10.1103/PhysRevE.86.021905)
15. Krogh A. 1919 The number and distribution of capillaries in muscles with calculations of the oxygen pressure head necessary for supplying the tissue. *J. Physiol.* (*Lond.*) **52**, 409–415. (doi:10.1113/jphysiol.1919.sp001839)
16. Rubenstein DA, Frame MD, Yin W. 2012 Biofluid mechanics. In *An introduction to fluid mechanics, macrocirculation, and microcirculation*. New York, NY: Academic Press.
17. Fang Q, Sakadzić S, Ruvinskaya L, Devor A, Dale AM, Boas DA. 2008 Oxygen advection and diffusion in a three-dimensional vascular anatomical network. *Opt. Express* **16**, 17 530–17 541. (doi:10.1364/OE.16.017530)
18. Schneider M, Reichold J, Weber B, Székely G, Hirsch S. 2012 Tissue metabolism driven arterial tree generation. *Med. Image. Anal.* **16**, 1397–1414. (doi:10.1016/j.media.2012.04.009)
19. Marbach S, Alim K, Andrew N, Pringle A, Brenner MP. 2016 Pruning to increase Taylor dispersion in *Physarum polycephalum* networks. *Phys. Rev. Lett.* **117**, 178103. (doi:10.1103/PhysRevLett.117.178103)
20. Sack L, Scoffoni C. 2013 Leaf venation: structure, function, development, evolution, ecology and applications in the past, present and future. *New Phytol.* **198**, 983–1000. (doi:10.1111/nph.12253)
21. Sack L, Streeter CM, Holbrook NM. 2004 Hydraulic analysis of water flow through leaves of sugar maple and red oak. *Plant Physiol.* **134**, 1824–1833. (doi:10.1104/pp.103.031203)
22. Coomes DA, Heathcote S, Godfrey ER, Shepherd JJ, Sack L. 2008 Scaling of xylem vessels and veins within the leaves of oak species. *Biol. Lett.* **4**, 302–306. (doi:10.1098/rsbl.2008.0094)
23. Price CA, Wing S, Weitz JS. 2012 Scaling and structure of dicotyledonous leaf venation networks. *Ecol. Lett.* **15**, 87–95. (doi:10.1111/j.1461-0248.2011.01712.x)
24. Jensen KH, Zwieniecki MA. 2013 Physical limits to leaf size in tall trees. *Phys. Rev. Lett.* **110**, 018104. (doi:10.1103/PhysRevLett.110.018104)
25. LaBarbera M. 1990 Principles of design of fluid transport systems in zoology. *Science* **249**, 992–1000. (doi:10.1126/science.2396104)
26. West GB, Brown JH, Enquist BJ. 1999 A general model for the structure and allometry of plant vascular systems. *Nature* **400**, 664–667. (doi:10.1038/23251)
27. Murray CD. 1926 The physiological principle of minimum work. *Proc. Natl Acad. Sci. USA* **12**, 299–304. (doi:10.1073/pnas.12.5.299)
28. Durand M. 2006 Architecture of optimal transport networks. *Phys. Rev. E* **73**, 016116. (doi:10.1103/PhysRevE.73.016116)
29. Bohn S, Magnasco MO. 2007 Structure, scaling, and phase transition in the optimal transport network. *Phys. Rev. Lett.* **98**, 088702. (doi:10.1103/PhysRevLett.98.088702)
30. Katifori E, Szöllosi GJ, Magnasco MO. 2010 Damage and fluctuations induce loops in optimal transport networks. *Phys. Rev. Lett.* **104**, 048704. (doi:10.1103/PhysRevLett.104.048704)
31. Corson F. 2010 Fluctuations and redundancy in optimal transport networks. *Phys. Rev. Lett.* **104**, 048703. (doi:10.1103/PhysRevLett.104.048703)
32. Ronellenfitsch H, Katifori E. 2016 Global optimization, local adaptation, and the role of growth in distribution networks. *Phys. Rev. Lett.* **117**, 138301. (doi:10.1103/PhysRevLett.117.138301)
33. Chang S-S, Tu S, Baek KI, Pietersen A, Liu Y-H, Savage VM, Hwang S-PL, Hsiai TK, Roper M. 2017 Optimal occlusion uniformly partitions red blood cells fluxes within a microvascular network. *PLOS Comp. Biol.* **13**, e1005892. (doi:10.1371/journal.pcbi.1005892)
34. Chan J, Bayliss PE, Wood JM, Roberts TM. 2002 Dissection of angiogenic signaling in zebrafish using a chemical genetic approach. *Cancer Cell.* **1**, 257–267.
35. Taylor G. 1953 Dispersion of soluble matter in solvent flowing slowly through a tube. *Proc. R. Soc. A* **219**, 186–203. (doi:10.1098/rspa.1953.0139)
36. Aris R. 1956 On the dispersion of a solute in a fluid flowing through a tube. *Proc. R. Soc. Lond. A* **235**, 67–77. (doi:10.1098/rspa.1956.0065)
37. Bruus H. 2001 *Theoretical microfluidics*. Oxford master series in physics, no. 18. Oxford, UK: Oxford University Press.
38. Lungu EM, Moffatt HK. 1982 The effect of wall conductance on heat diffusion in duct flow. *J. Eng. Math.* **16**, 121–136. (doi:10.1007/BF00042550)
39. Graetz L. 1882 Über die wärmeleitungsfähigkeit von flüssigkeiten. *Ann. Phys.* **254**, 79–94. (doi:10.1002/andp.18822540106)
40. Datta S, Ghosal S. 2008 Dispersion due to wall interactions in microfluidic separation systems. *Phys. Fluids* **20**, 012103. (doi:10.1063/1.2828098)
41. Hemida HN, Sabry MN, Abdel-Rahim A, Mansour H. 2002 Theoretical analysis of heat transfer in laminar pulsating flow. *Int. J. Heat Mass Transf.* **45**, 1767–1780. (doi:10.1016/S0017-9310(01)00274-5)
42. Zwieniecki MA, Melcher PJ, Boyce CK, Sack L, Holbrook NM. 2002 Hydraulic architecture of leaf venation in *Laurus nobilis* L. *Plant Cell Environ.* **25**, 1445–1450. (doi:10.1046/j.1365-3040.2002.00922.x)
43. Roth-Nebelsick A, Uhl D, Mosbrugger V, Kerp H. 2001 Evolution and function of leaf venation architecture: a review. *Ann. Bot.* **87**, 553–566. (doi:10.1006/anbo.2001.1391)
44. Jensen KH, Rio E, Hansen R, Clanet C, Bohr T. 2009 Osmotically driven pipe flows and their relation to sugar transport in plants. *J. Fluid Mech.* **636**, 371–396. (doi:10.1017/S002211200900799X)
45. Holbrook NM, Zwieniecki MA. 2011 *Vascular transport in plants*. New York, NY: Academic Press.

46. Fricker M, Willmer C. 2012 *Stomata*. Berlin, Germany: Springer Science & Business Media.
47. Cha P, Alim K, Brenner MP. In preparation. Absorption in a dilating tube and its implication for blood flow.
48. Ronellenfitsch H, Lasser J, Daly DC, Katifori E. 2015 Topological phenotypes constitute a new dimension in the phenotypic space of leaf venation networks. *PLoS. Comput. Biol.* **11**, e1004680. (doi:10.1371/journal.pcbi.1004680)
49. Thorne ET, Young BM, Young GM, Stevenson JF, Labavitch JM, Matthews MA, Rost TL. 2006 The structure of xylem vessels in grapevine (Vitaceae) and a possible passive mechanism for the systemic spread of bacterial disease. *Am. J. Bot.* **93**, 497–504. (doi:10.3732/ajb.93.4.497)
50. Sack L, Scoffoni C, McKown AD, Frole K, Rawls M, Havran JC, Tran H, Tran T. 2012 Developmentally based scaling of leaf venation architecture explains global ecological patterns. *Nat. Commun.* **3**, 837. (doi:10.1038/ncomms1835)
51. Vico G, Manzoni S, Palmroth S, Katul G. 2011 Effects of stomatal delays on the economics of leaf gas exchange under intermittent light regimes. *New Phytologist* **192**, 640–652. (doi:10.1111/j.1469-8137.2011.03847.x)
52. Woodward FI, Kelly CK. 1995 The influence of CO_2 concentration on stomatal density. *New Phytologist* **131**, 311–327. (doi:10.1111/j.1469-8137.1995.tb03067.x)
53. Phillips R. 2013 *Physical biology of the cell*, 2nd edn. London, UK: Garland Science, Taylor & Francis Group.
54. van Bel AJ, Mostert E, Borstlap AC. 1979 Kinetics of L-alanine escape from xylem vessels. *Plant Physiol.* **63**, 244–247. (doi:10.1104/pp.63.2.244)
55. Horwitz L. 1958 Some simplified mathematical treatments of translocation in plants. *Plant Physiol.* **33**, 81–93. (doi:10.1104/pp.33.2.81)
56. Durand M. 2007 Structure of optimal transport networks subject to a global constraint. *Phys. Rev. Lett.* **98**, 088701. (doi:10.1103/PhysRevLett.98.088701)
57. Banavar JR, Colaiori F, Flammini A, Maritan A, Rinaldo A. 2000 Topology of the fittest transportation network. *Phys. Rev. Lett.* **84**, 4745–4748. (doi:10.1103/PhysRevLett.84.4745)
58. Alvarez S, Marsh EL, Schroeder SG, Schachtman DP. 2008 Metabolomic and proteomic changes in the xylem sap of maize under drought. *Plant Cell Environ.* **31**, 325–340. (doi:10.1111/j.1365-3040.2007.01770.x)
59. Eilmann B, Zweifel R, Buchmann N, Fonti P, Rigling A. 2009 Drought-induced adaptation of the xylem in Scots pine and pubescent oak. *Tree Physiol.* **29**, 1011–1020. (doi:10.1093/treephys/tpp035)
60. Canny MJ, Sparks JP, Huang CX, Roderick ML. 2007 Air embolisms exsolving in the transpiration water the effect of constrictions in the xylem pipes. *Funct. Plant Biol.* **34**, 95–111. (doi:10.1071/FP06210)
61. Lovisolo C, Schubert A. 1998 Effects of water stress on vessel size and xylem hydraulic conductivity in *Vitis vinifera* L. *J. Exp. Bot.* **49**, 693–700. (doi:10.1093/jxb/49.321.693)